The Massachusetts Toxics Use Reduction Institute
University of Massachusetts Lowell

Improved Lead-Free Wire and Cable Insulation Performance Using Nanocomposites

Toxics Use Reduction Institute
University Research in Sustainable Technologies Program

Technical Report No. 58 2006

University of Massachusetts Lowell

Improved Lead-Free Wire and Cable Insulation Performance Using Nanocomposites

Noble Francis and Dr. Daniel Schmidt
Department of Plastics Engineering
University of Massachusetts Lowell

The Toxics Use Reduction Institute
University Research in Sustainable Technologies Program

The Toxics Use Reduction Institute
University of Massachusetts Lowell

2006

The Massachusetts Toxics Use Reduction Institute
University of Massachusetts Lowell

All rights to this report belong to the Toxics Use Reduction Institute. The material may be duplicated with permission by contacting the Institute.

The Toxics Use Reduction Institute is a multi-disciplinary research, education, and policy center established by the Massachusetts Toxics Use Reduction Act of 1989. The Institute sponsors and conducts research, organizes education and training programs, and provides technical support to promote the reduction in the use of toxic chemicals or the generation of toxic chemical byproducts in industry and commerce. Further information can be obtained by writing the Toxics Use Reduction Institute, University of Massachusetts Lowell, One University Avenue, Lowell, Massachusetts 01854.

©Toxics Use Reduction Institute, University of Massachusetts Lowell

University Research in Sustainable Technologies

The University Research in Sustainable Technologies program is a project of the Toxics Use Reduction Institute (TURI). The program taps the research capabilities of the University of Massachusetts to advance the investigation, development and evaluation of sustainable technologies that are environmentally, occupationally and economically sound. The program provides research funding to UMass faculty from all campuses, annually, on a competitive basis and encourages faculty/industry partnerships and cross-campus collaboration. Industry partners provide guidance, propose applications for new technologies and, in some cases, evaluate and/or adopt processes and technologies resulting from research.

Past projects supported by this program have focused on finding alternatives to the use of toxic chemicals in the wire and cable industry. These projects, which are described in more detail on TURI's website (go to www.turi.org and click on Industry, Research, University Research in Sustainable Technologies, Wire and Cable Projects), include:

- **2005** - Flame Retardancy Enhancement for EPDM Wire and Cable Coatings Using Nanoclays – Prof. Joey Mead, UMass Lowell Department of Plastics Engineering.
- **2004** - Alternative Stabilizers and Surface Characterization (SEM/EDXS Analysis) of EPDM for Wire and Cable Applications – Prof. Joey Mead, UMass Lowell Department of Plastics Engineering, and Changmo Sung, UMass Lowell Department of Chemical Engineering.
- **2003** - Analysis of Lead-Containing Wire Coating Materials – Prof. Joey Mead, UMass Lowell Department of Plastics Engineering, and Changmo Sung, UMass Lowell Department of Chemical Engineering.
- **2003** - Innovative Materials for Wire and Cable Coating – Prof. Stephen McCarthy, UMass Lowell Department of Plastics Engineering and the Institute for Plastics Innovations.
- **2002** - Innovative Materials for Wire and Cable Coating – Prof. Stephen McCarthy, UMass Lowell, Department of Plastics Engineering and the Institute for Plastics Innovations.

Notice

This report has been reviewed by the Institute and approved for publication. Approval does not signify that the contents necessarily reflect the views and policies of the Toxics Use Reduction Institute, nor does the mention of trade names or commercial products constitute endorsement or recommendation for use.

Executive Summary

The goal of this project is the production of high-performance, low-cost lead-free PVC compounds for wire and cable insulation, to address the serious environmental issues surrounding the use of their leaded counterparts and the lack of market acceptance of current alternatives to PVC. Clay nanocomposite technology has been chosen as a means to achieve this goal, as it has been demonstrated that such systems can improve a variety of properties relevant to the performance of wire and cable insulation (thermal stability, barrier properties, flame retardance, etc.). Here we report on the characterization of transparent, lead-free PVC nanocomposites produced by melt blending with organoclay loadings of 2, 5, and 10 wt%. Structural studies carried out via x-ray diffraction indicate significant intercalation as well as orientation of the clay sheets in the flow direction. From MOCON testing, nanocomposites with 2 wt% clay showed a five-fold increase in oxygen barrier. While a substantial improvement in thermal stability was not observed in TGA experiments, the greatly improved oxygen barrier properties may nevertheless enhance thermal stability in real-world settings. From mechanical properties testing, the modulus of the PVC/nanocomposite was found to increase with clay content; nevertheless, 2 wt% was found to be the optimal loading level due to the degradation of ultimate properties with higher clay content.

Table of Contents

Project Background – Relevance to Sustainability

Lead salts are currently used as stabilizers in chlorinated polyethylene and poly (vinyl chloride) formulations for wire and cable insulation. According to 1999 TURA data[1], the insulation industry in Massachusetts alone used nearly 3.5 million pounds of lead compounds – A serious environmental concern for industry in our state, not to mention the country as a whole. Alternatives to these compounds are often themselves quite toxic, and include barium and cadmium salts and organotin compounds. Likewise, increased cost and/or reduced performance in alternative formulations limit their practical acceptance. Nevertheless, some lead-free, low toxicity alternatives are currently on the market; Teknor Apex, a Massachusetts-based compounder of PVC resins, for instance, announced in May 2005 that is has "the broadest range of non-lead stabilized (NLS) vinyl compounds available to the wire and cable industry, enabling companies to manufacture products that comply with the European Union's upcoming 'RoHS' legislation".

While an eventual phase-out of chloropolymers represents a long-term goal, the objective of this work is to take these new, lead-free compositions, and further enhance their performance and practical utility through the addition of a small amount of organically modified clay, to form a layered silicate nanocomposite – an approach that, once validated, will have future utility in non-PVC based formulations as well. The idea is to take advantage of an effect already demonstrated commercially by Honeywell's Aegis nanocomposite barrier resins[2]. The barrier component of these resins is polyamide containing both organically modified clay and an oxygen scavenger. Dispersed clay platelets alone improve barrier properties thanks to their high aspect ratio and impermeability, which forces diffusing species to take a highly tortuous path in order to pass through the material. Oxygen scavengers, on the other hand, chemically consume oxygen as it attempts to diffuse through the material. While neither one gives an oxygen permeability low enough to compete with glass, when combined, they do exactly that, thanks to a synergistic effect. Simply put, the longer diffusion path the clay forces the oxygen to take greatly improves the chances that oxygen and oxygen scavenger will meet, while giving the oxygen scavengers more time to do their work.

In the case of wire and cable insulation, PVC-based compositions thermally degrade by "zip dechlorohydration", a shown below[3].

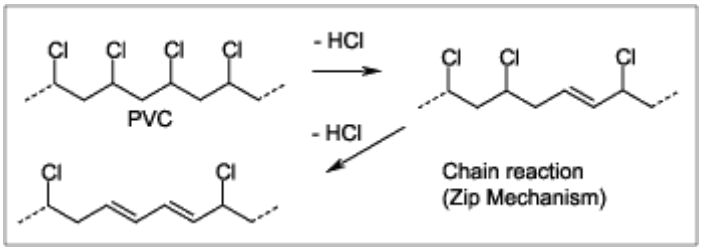

Structural defects in the PVC and the presence of oxygen, acids or bases (including HCl itself) both accelerate this degradation. This effect is readily apparent; discoloration of the polymer occurs as numerous double bonds are formed and highly conjugated molecules appear. Such highly conjugated molecules, in turn, tend not only to have increased electrical conductivity compared to the original polymer, but are also very sensitive to oxidative degradation. The end result is a dramatic degradation in the physical, mechanical, and electrical properties of the insulation material.

Stabilizers slow this process by coupling with defects or double bonds formed as a result of dechlorohydration, by scavenging acids or bases from the system, or by acting as antioxidants.

The addition of clays to such a system allows for a number of specific enhancements with respect to what such stabilizers already accomplish. From the aforementioned case of the Nylon-6 oxygen barrier films, it is clear that dispersed clays can increase scavenging efficiency; the same effects with respect to HCl scavenging can therefore be expected here. Likewise, the cationic surfactants that are ion-exchanged into the interlayer galleries of the clays can be chosen for double duty, not only helping to disperse the clay in the polymer (their primary function), but also serving as antioxidants themselves, through inclusion of unsaturated functionalities, further enhancing the thermal stability of these materials. Finally, in addition to the enhanced thermal stability often seen in polymer/clay nanocomposites in general, an additional advantage often seen in these systems is their inherent flame retardance, due to formation of silicate char once burning begins at an exposed surface.

These factors give the producer some attractive choices. Thermal stability and flame retardance may be improved, and the overall performance of the formulation therefore enhanced, without addition of the primary stabilizer. Alternatively, if the performance is already acceptable without the clays, their addition may allow for a reduction in the concentration of primary stabilizer, which could result in reduced costs and/or issues of toxicity, depending on the compound in use. Finally, amounts of flame-retardants might also be reduced in nanocomposite formulations.

At this point, one may ask why it is even necessary to pursue such ends, if lead-free formulations are already available. According to industry experts, performance of the lead-free systems is not yet on par with that of lead-based systems, and enhanced performance in the lead-free systems would definitely improve their market acceptance. This raises an important point: It is not enough simply to produce such materials; they must be accepted and used as widely as possible to facilitate the elimination of leaded formulations.

Research Objectives

Polymer nanocomposites represent a new and promising area of polymer research. Among the particles used to form nanocomposites, organically modified clays are of particular interest. In such systems, the combination of high aspect ratio clay mono- or multi-layers and their interactions with the matrix polymer can lead to improvements in barrier, thermal, and mechanical properties at far lower loading levels than are typically used in conventional filled polymer composites[4, 5, 6].

In this work we seek to produce lead-free PVC nanocomposites with different levels of clay loading and investigate improvements in properties related to thermal stability while retaining the mechanical flexibility and toughness required for wire and cable applications, with the goal of making the properties of lead-free PVC formulations more competitive and their use more accepted as a result. We investigate the structure (via x-ray diffraction), barrier, thermal and mechanical properties of melt-blended PVC nanocomposites, and report on the development of a new PVC/clay masterbatching technique that may improve clay dispersion when combined with compatible systems and reduce dust issues associated with clay handling.

The overall objective of this work is to enhance the properties and/or reduce the costs of the environmentally preferable lead-free wire and cable insulation formulations available commercially in order to address the issue of poor market acceptance vs. the far more toxic lead-

based systems. In the absence of strong government oversight, the production of lead-free alternatives is only part of the solution; only when such alternative formulations are widely used will the issue of lead in wire and cable insulation be properly addressed.

Experimental

Materials

A lead-free high flow injection molding grade PVC (3006-90 Clear 0217) was procured from AlphaGary and was used as received (denoted as *R1* in Appendix A) in the form of clear, colorless pellets).

Two organophilic montmorillonite (OMMT) clays were chosen for study – Southern Clay's Cloisite 30B (denoted as *Clay1* in Appendix A) and Cloisite 10A products (denoted as *Clay2* in Appendix A) – and used as received (in the form of beige, free-flowing powders).

Clay1 was chosen for evaluation based on numerous literature reports indicating excellent compatibility with PVC and improved thermal and mechanical properties in melt-blended systems[7, 8, 9, 10, 11, 12, 13, 14]. *Clay1* consists of montmorillonite layers modified by the methyl tallow bis (2-hydroxyethyl) ammonium cation (MT2EtOH).

Clay2 was chosen for evaluation based on the similarity of its dimethylbenzyl (hydrogenated tallow) ammonium (2MBHT) modifier to the MT2EtOH modifier of *Clay1*, coupled with the presence of aromatic substituents for added thermal stability and/or antioxidant properties and at least one report of compatibility with PVC[15]. It was found, however, that the presence of free 2MBHT modifier in *Clay2* (~36% in excess of the ion-exchange capacity of the unmodified clay, vs. no excess in the case of *Clay1*[16]) enhanced thermal degradation to such a degree that the materials were unusable. This observation is consistent with the ability of free quaternary ammonium salts to catalyze the dechlorohydration of PVC[17, 18]; the success of the aforementioned study[15] is attributed to the extraction of the excess modifier during solution polymerization of PVC and subsequent washing prior to melt compounding.

Initially a low viscosity plasticizer, PLASTHALL® DOS (dioctyl sebacate) was selected and combined with *Clay1* at levels of up to 35 wt%. Since then a plasticizer more relevant to wire and cable formulations, DIDP (diisodecyl phthalate), has been provided by our industrial partner as more appropriate for wire and cable compounds based on its higher thermal stability and decreased volatility, with results from this new plasticizer system. Results reported here are based on the use of DINP as the sole plasticizer. The compatibility of *Clay1* with DIDP has also been observed to be greater than with DOS, based on the higher OMMT loadings achievable in DIDP vs. DOS in spite of the higher viscosity of the former, likely due to the affinity of the polar silicate surface for the more polar phthalate functionality vs. the less polar sebacate functionality.

For added clarity, chemical structures for the *Clay1* and *Clay2* modifiers as well as DOS and DIDP are shown in Figure 1. Note that in the free form the clay modifiers are present as chloride salts, while in the ion-exchanged form negative charges from the clay layers acts as counter-ions instead. In the latter case the chloride is no longer present and the modifiers are no longer able to move independently of the clay layer.

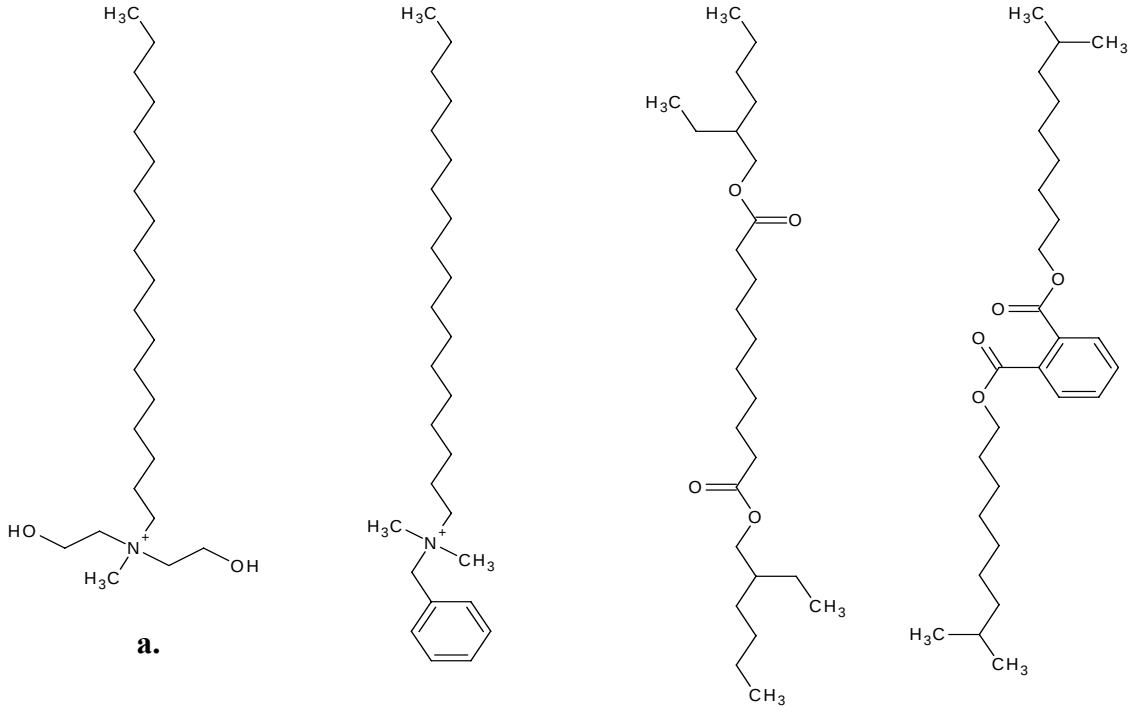

Figure 1. Chemical structures of the Cloisite 30B (*Clay1*) **(a.)** and 10A (*Clay2*) **(b.)** modifiers and of the PVC plasticizers dioctyl sebacate, DOS **(c.)** and diisodecyl phthalate, DIDP **(d.)**

Preparation of PVC /OMMT Nanocomposites – "Conventional Blending"

The commercial PVC pellets *R1* were dry blended with *Clay1* and *Clay2* in a Twin shell dry blender for a fixed time of 15 minutes. Since the speed of rotation could not be changed the dry blends were rotated at a constant rotational speed of 25 RPM. The blends were prepared with *Clay1* at OMMT loadings of 2, 5 and 10 wt % (Samples *Ae*, *Be* and *Ce* in Appendix A) and with *Clay2* at 2, 5 and 10 % loading level (Samples *Ke*, *Le*, *Me*). A batch size of 1.5 kg was used, this being the smallest size that allowed for practical processing and produced sufficient materials for further tests.

The mixed granules were then extruded in a twin screw extruder (Werner Pfliederer/W&P 30 mm, L/D = 32). The nanocomposite emerged from the extrusion die in the form of long strands or ropes which were allowed to cool, then granulated to produce small cylindrical pellets a few millimeters in diameter. The temperature zones of the extruder from the hopper to the die were maintained at 90, 150, 160, 170, and 180 °C, respectively, while the screw speed was set at 40 RPM.

Preparation of OMMT/Plasticizer Masterbatches

Plasticizer/OMMT blends ("masterbatches") intended for subsequent mixing with the PVC resin pellets were prepared via the following three methods, with the emphasis (in 1 and 2) on maximizing OMMT content:

1) *Clay1* was slowly added to DIDP plasticizer in a large beaker via manual stirring, producing masterbatches (blending process MB-C2P in Appendix A) with up to 40 wt% of *Clay1*.

2) Cloisite 30B was combined directly with DIDP plasticizer in a FlackTek DAC-150 FVZ-K high speed mixer rotating at 3000 RPM for one minute, producing masterbatches (blending process MB-SM in Appendix A) with up to 45 wt% of *Clay1*.

3) 37.5 g of DIDP plasticizer was added slowly to 40 g of *Clay1* and was stirred manually in order to produce a ~50 wt% OMMT masterbatch specifically intended to produce nanocomposites with 2 wt% overall OMMT loading when working with 2 kg nanocomposite batch sizes (blending Process MB-P2C in Appendix A).

For all the three trials the masterbatch was mixed until it was observed to be homogeneous and its form allowed it to be readily combined with the PVC granules.

Preparation of PVC/Masterbatch Blends

Three trials were carried out using the three types of masterbatches described above, which were each mixed with the PVC such that the overall percentage of OMMT was 2 wt%.
This was accomplished in a twin shell dry blender run for 15 minutes at 25 RPM.

The granules were then extruded in a twin screw extruder (Werner Pfliederer/W&P 30 mm, L/D = 32) as per the procedures listed for conventional blending (Samples *G*, *H*, *I* in Appendix A).

Sheet Extrusion of Conventional Blended PVC/OMMT Nanocomposites

Extruded PVC/OMMT granules produced via conventional blending were used for the production of extruded sheet. Only the 2 and 5 wt% nanocomposites (Samples *Ase*, *Bse* in Appendix A) were used for this purpose, the 10 wt% formulation (Sample *Cse*) producing inhomogeneous sheet due to its greater viscosity and propensity for thermal degradation. These sheets were then analyzed with respect to their barrier properties, with pure PVC (Sample *Jse*) also extruded as a reference sample.

Sheet extrusion was carried out on a Welex single screw extruder. A temperature profile of 90, 150, 160, 170, 175, 175, 180, and 180 °C was maintained from feed throat to sheet die. The cooling rolls were kept at 24-25 °C while the screw speed was set at 17 RPM. Thicknesses of the sheet samples obtained have been indicated in Table 2.

Injection Molding of Conventional Blended PVC/OMMT Nanocomposites

Extruded PVC/OMMT granules (2, 5 and 10 wt% loading) produced via conventional blending (Samples *Ae, Be* and *Ce*) and pure PVC (Sample *Je*) were used for the production of injection-molded bars (Samples *Aim, Bim and Cim* in Appendix A). These bars were then analyzed via x-ray diffraction.

Tensile and heat deflection bars were molded on a 55-ton injection molding machine. The temperatures used, from zone 1 to die, were 150, 160, 165, and 170 °C for the *Je* pure PVC and *Ae* OMMT nanocomposite, and were increased by 10 °C for *Be* and *Ce* OMMT nanocomposites to ensure complete filling of the mold.

X-ray Diffraction Analysis: Reflection Geometry, Point Detector

X-ray diffraction measurements were carried out using Cu K_α radiation (λ = 0.15418 nm) at a scanning rate of 1°/min from 1-10° 2θ. A scintillation detector was used to measure the diffracted intensity. Bragg's Law, $2d \sin\theta = n\lambda$, was used to calculate the interlayer spacing. The specimens used for these studies were 1" × ½" pieces cut from injection-molded bars from Samples *Aim, Bim, Cim* and *Jim*. The diffraction geometry is shown in Figure 2.

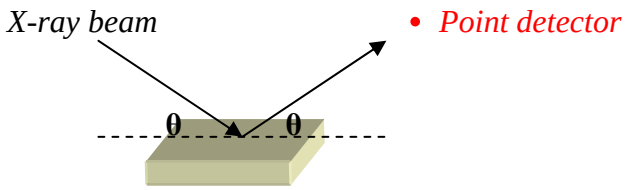

Figure 2. Schematic of Reflection Geometry XRD with Point Detector

X-ray Diffraction Analysis: Transmission Geometry, Area Detector

X-ray diffraction measurements were carried out using a Bruker Instruments D8 DISCOVER/GADDS system (Air Force Research Labs, Wright-Patterson AFB). Two dimensional diffraction patterns were generated during the course of a one hour scan on each sample (40 kV, 40mA, Cu K_α radiation, λ = 0.15418 nm). The x-ray beam center was calibrated using a silver behenate low-angle diffraction standard. The integrated data (i.e. 2θ and azimuthal scans) derived from the two dimensional diffraction images were produced using the FIT2D software. Plotting and peak-fitting were carried out in Microcal Origin, a scientific plotting and analysis package. The specimens used for these studies were *Aes* and *Bes*, thin strips cut three at a time from the extruded sheet samples (2 and 5 wt% nanocomposites only), adhered together using double-sided tape, and mounted edge-on. Three sheets were used to ensure that the width of the sample would always exceed the width of the x-ray beam, obviating the need to account for the exact thickness of the sheet from sample to sample. The amount of material through which the beam traveled was measured with digital calipers to be 0.6 mm in all cases, with a maximum variation of 10%.

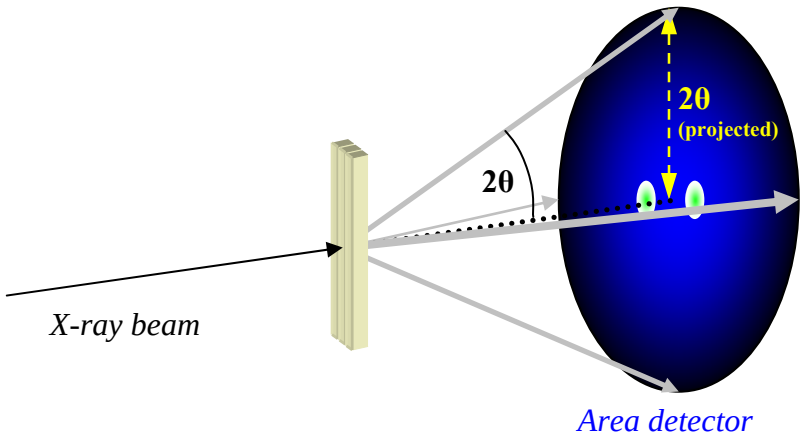

Figure 3. Schematic of Transmission Geometry XRD with Area Detector

Permeability Testing

Extruded sheet samples of ***Jse*** and two nanocomposites (***Ase*** and ***Bse***, respectively) produced from conventionally blended granulate were cut and sent to the U. S. Army Soldier Systems Center (Natick, MA) for permeability testing (see sheet thicknesses given in Table 2). The oxygen permeation rate was measured on a MOCON permeation instrument at 65% relative humidity at 24°C. The permeation rate is defined as follows:

$p = qt / aT$

Where p = Permeation rate
q = Quantity of permeant
t = Film thickness
a = Area over which permeation is occurring
T = Time taken for permeation

Note that while T depends on sample dimensions, p does not.

Thermogravimetric Analysis (TGA)

Thermal decomposition studies were performed in air over a temperature range of 50-600 °C using a TGA 2950 (TA Instruments) at a scan rate of 10 °C/min. Samples *Je, Ae* and *Be* extruded granulate of the pure PVC its 2 and 5 wt% OMMT nanocomposites produced via twin screw extrusion (conventional blending) were used for these studies.

Mechanical testing

Tensile tests were carried out on an Instron tensile testing machine (Model 4400) according to ASTM D412. A load cell of 50 pounds was used for these experiments. The cross head speed was set at 50 mm/min and the gauge length was fixed at 40mm. The tensile specimens were cut to the required dimensions from extruded sheet produced on the sheet extruder Samples *Ase, Bse* and *Jse.* The test was carried out at room temperature (25 °C). Ten samples were tested in machine direction and ten samples were tested in the transverse direction as per ASTM D412. The average dimensions of these specimens were 100 mm long by 7 mm wide by 0.4 mm thick.

Results and Discussion

Sheet Extrusion

The continuously extruded pure PVC sheets (Sample *Jse*) had thicknesses in the range of 16-33 mil, while the *Ase* and *Bse* samples had thicknesses in the range of 8.5-18 mil with some slight variation in thickness vs. the length and width of the sheets (see Table 2 for representative dimensions). Approximately 20 feet of the sheet was extruded. Materials limitations at the time prevented further studies on achievable sheet thickness. While all sheets were transparent, it should be noted that Sample *Jse* possessed only a single process history (sheet extrusion only), versus Samples *Ase* and *Bse*, which were processed twice (twin screw extrusion then sheet extrusion).

OMMT/Plasticizer Masterbatching

One goal of the research was to prepare appropriate OMMT/plasticizer masterbatches that would mix homogeneously with PVC resin pellets to give improved OMMT dispersion and materials handling characteristics (i.e. lower dust levels). These masterbatches were made successfully using three different techniques as mentioned above.

While mixing PVC with the OMMT/plasticizer masterbatches obtained from techniques 1 and 2 in the twin shell blender, it was observed that the PVC granules began to clump and stick to one another. The masterbatch itself also tended to agglomerate and adhere to the surface of the vessel, reducing the overall amount of OMMT retained by the PVC granulate and incorporated during twin screw extrusion *(*Samples *G* and *H).* An attempt to remedy this problem by freezing the masterbatch in liquid nitrogen was unsuccessful due to rapid thawing of the frozen masterbatch in the twin-shell mixer.

The masterbatch prepared according to technique 3 , being more solid-like in character than the aforementioned materials, was found to be more useful thanks to its more solid-like character, which prevented the aforementioned problems of clumping and adhesion. Upon mixing with the PVC pellets only a small amount of the masterbatch was found to remain on the inner surface the surface of the twin shell blender and without any agglomeration. The mixture was then melt compounded via twin screw extrusion (Sample *I*).

The granules obtained were found to be darker in color and less transparent than those produce via conventional PVC/*Clay1* nanocomposite blending. A lack of transparency in a formerly transparent material is indicative of the formation of domains capable of scattering light, implying some degree of phase-separation in this system. While this lack of compatibility is disappointing, it is likely that DIDP is not well-matched with the PVC formulation used for this work due to the exact nature of the plasticizers and additives it already contains.

With that in mind, the development of a practical means of not only producing plasticizer/OMMT masterbatches but of combining them with polymer via twin screw extrusion is indeed promising for future work so long as the plasticizer chosen for the masterbatch is compatible with that already present in the resin. This plasticizer/OMMT masterbatch technique may also provide a means of reducing dust levels during processing, given the visible increase in particle size and more solid-like, less powdery character of the masterbatches produced here vs. the original, free-flowing OMMT powder.

At this point it should be noted that the *Clay1* as delivered, are free-flowing powders of micron-sized particles (90% <13 μm, 50% <6 μm, 10% <2 μm)[19]; nanoparticles are only produced when these particles are mechanically mixed in a compatible viscous medium. Instead, the primary dust hazard associated with this *Clay1* is due to the presence of (<0.5%) crystalline silica (quartz) found naturally in these types of clays and known to cause silicosis as a result of chronic exposure by inhalation[20]. While the magnitude of this hazard is reduced by the low concentration quartz in the OMMT (also necessary to preserve nanocomposite properties, as such inclusions can act as points of mechanical failure), plasticizer masterbatching should nevertheless allow for even further reductions in airborne quartz concentration.

X-ray Diffraction Analysis: Reflection Geometry, Point Detector

X-ray diffraction (XRD) was used to characterize the layered structure of the PVC/OMMT nanocomposites; changes in the 2θ values of the low-angle diffraction peaks indicate changes in the spacing between individual clay layers. Figure 4 shows the x-ray diffraction pattern of the *Clay1* used

in this study. The characteristic diffraction peak d_{001} is located at around 4.7°, corresponding to a basal interlayer spacing of 1.9 nm according to Bragg's Law.

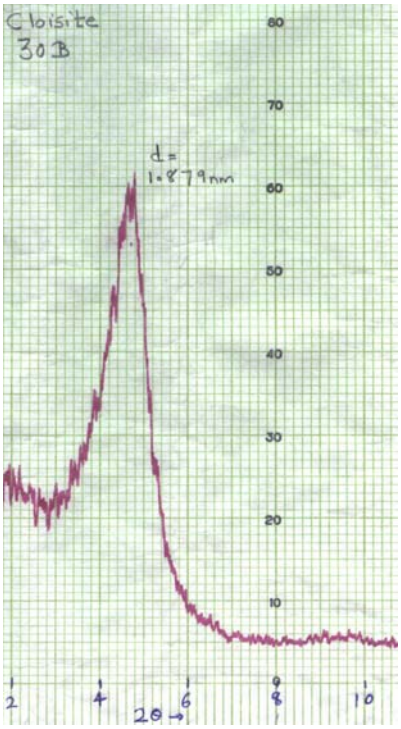

Figure 4. XRD Pattern of *Clay1* (Pure Cloisite 30B)

Figure 5a., b., and c. display the diffraction patterns of cut, injection molded PVC/OMMT nanocomposites bars containing 2 wt%, 5 wt% and 10 wt% of OMMT (Samples *Aim, Bim, Cim*), respectively. As shown here, the characteristic diffraction peak of the OMMT decreases significantly in intensity and increase in broadness. It also shifts to lower angles, indicating that the interlayer spacing of the *Clay1* has been expanded versus the *Clay1* alone.

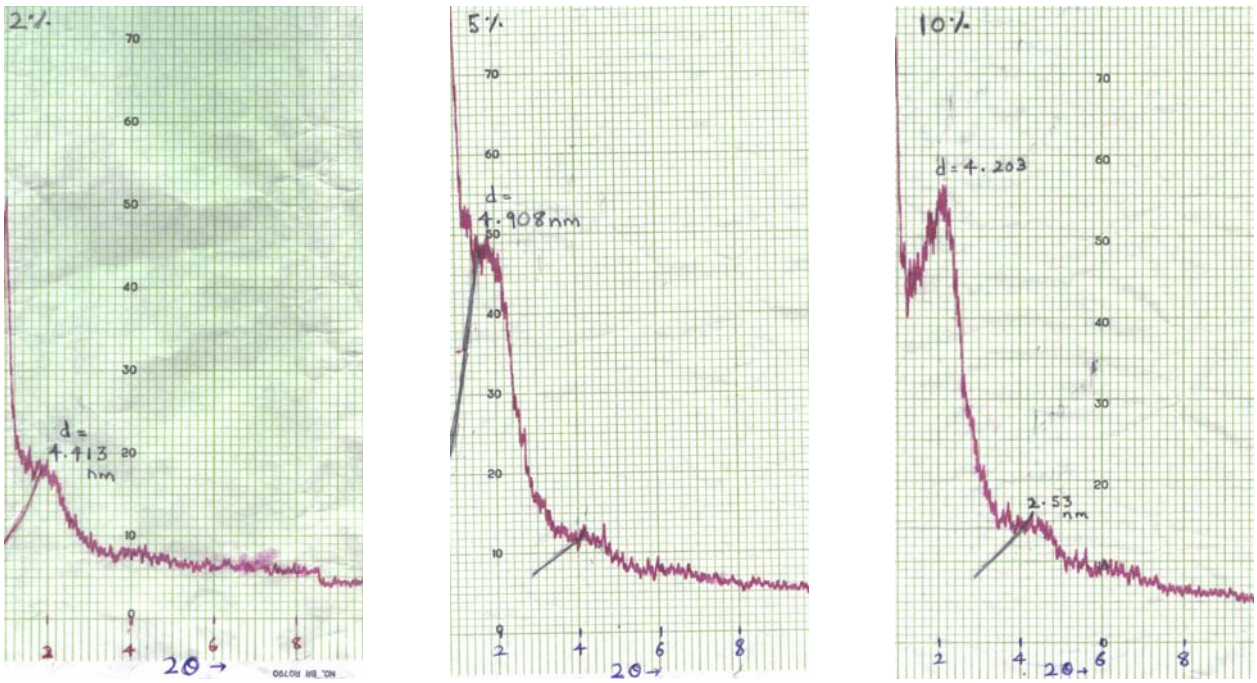

Figure 5. X-ray diffraction patterns of Samples *Aim* (a.), *Bim* (b.), & *Cim* (c.)

In the case of Sample *Aim* the new peak position (2θ = 2.0°) corresponds to a gallery spacing of 4.4 nm. While inconclusive in the absence of other data, the observed significant decrease in intensity accompanied by the broadening of the peak is nevertheless consistent with partial exfoliation of some *Clay1* sheets from *Clay1* stacked layers. In x-ray diffraction, peak broadening is a direct result of a reduction in the average size of the scattering domains in a sample. In this case, the reduction in size of the multilayer clay stacks is explained by a reduction in stack thickness due to delamination. Likewise, a reduction in diffraction intensity is a direct result of a lower concentration of properly oriented scattering domains in the path of the x-ray beam. In the context of the nanocomposites being studied this can be explained by a loss of parallel registry and/or even spacing between individual sheets, both of which would be expected in exfoliated systems.

In the case of Sample *Bim* the intensity of the peak is less affected, while the peak location is read as 2θ = 1.8°, corresponding to a gallery spacing of 4.9 nm, with a second order diffraction peak now visible as well. A similar trend is observed with Sample *Cim*, where the basal spacing is increased to 4.2 nm and the second order diffraction peak is more apparent.

Table 1. XRD Results from OMMT and PVC / OMMT Nanocomposites

Sample ID	Sample Composition	2θ	d-spacing (nm)	Nanostructure
Clay 1	OMMT	4.7°	1.9	Unintercalated
Aim	PVC + 2 wt% OMMT	2.0°	4.4	Intercalated
Bim	PVC + 5 wt% OMMT	1.8°	4.9	Intercalated
Cim	PVC + 10 wt% OMMT	2.1°	4.2	Intercalated

Overall, these results indicate that the PVC resin has intercalated into the interlayer galleries of the OMMT and confirm compatibility between the two, with the potential left open for some degree of exfoliation as well, especially in the Sample *Aim*. Conclusions beyond this are not offered due to the difficulty in assigning accurate peak positions at such low angles and in the presence of a significant background signal. Table 1 summarizes these results.

X-ray Diffraction Analysis: Transmission Geometry, Area Detector

The D8 DISCOVER with GADDS can be used for nanostructure analysis including particle shape, size, distribution and particle orientation. The false color images obtained by the instrument can give us a very good idea of the orientation in the samples. If there is a preferred orientation in terms of rotation about the beam axis, we will see some areas of the ring become stronger and others become weaker. Note that the data shown here come from extruded film samples mounted edge on, with the plane of the film corresponding to the vertical axis of the images shown.

Figures 5 and 6 make this idea more clear. Here the ring is visible to the left and right of the center point, indicating that almost all of the clay layers present in the form of multilayer stacks are oriented parallel to the beam direction and in the plane of the extruded film being analyzed. The diffracted intensity is higher in Sample *Bse*, where second-order diffraction becomes visible, though it should be noted that this is attenuated some due to increased sample thickness.

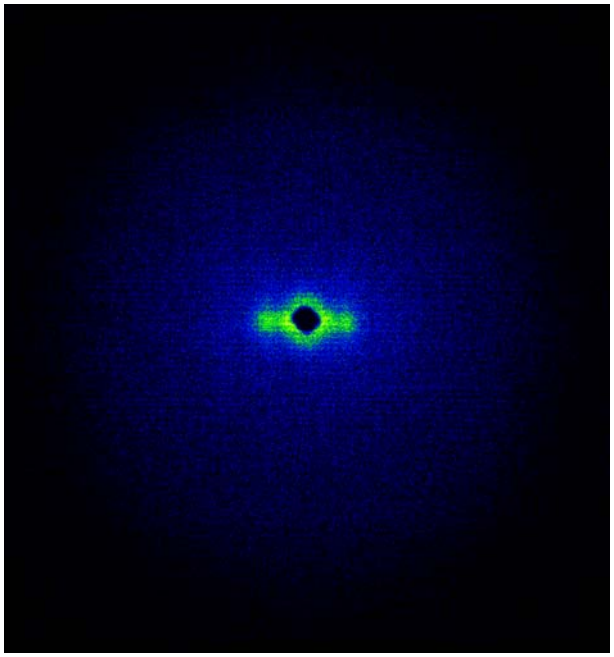

Figure 5. Diffraction rings in Sample *Ase* (PVC + 2 wt% Cloisite 30B)

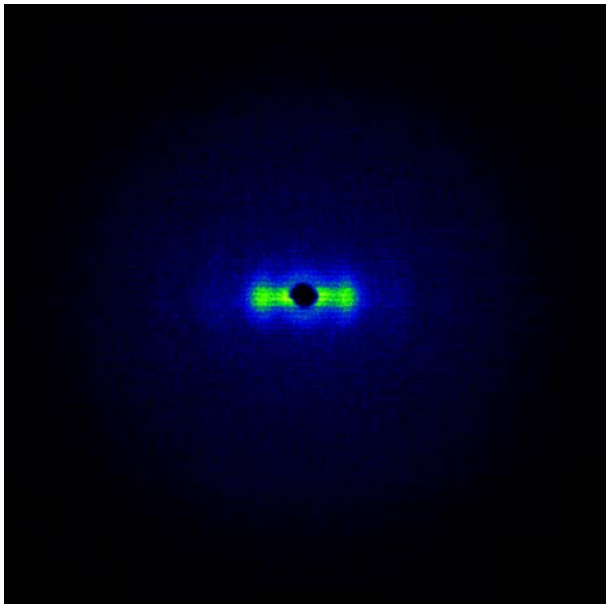

Figure 6. Diffraction rings in Sample ***Bse*** (PVC + 5 wt% Cloisite 30B)

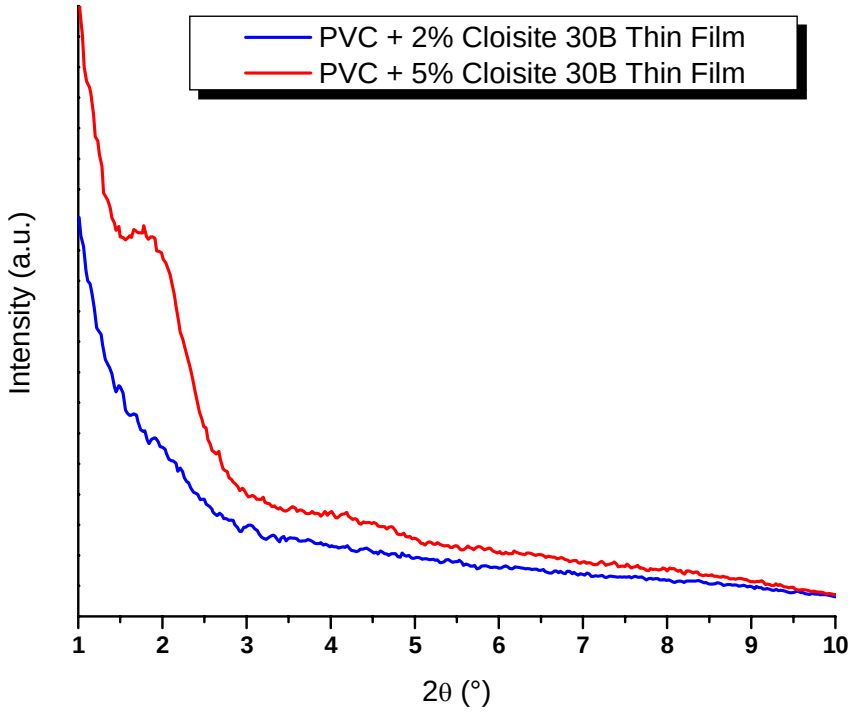

Figure 7. Integrated intensity (arbitrary units) vs. 2θ (°) for PVC NC thin films samples ***Ase*** (blue) and ***Bse*** (red).

Figure 7 shows the plot of diffracted intensity vs. 2θ obtained by integrating the 2-D diffraction pattern; note that 2θ corresponds to distance from the center in the 2-D pattern. Here the first order diffraction peak of the intercalated structure is clearly visible in the Sample *Bse* nanocomposite, but very weak in nanocomposite. With that said, it is important to note that the peak in the Sample *Ase* nanocomposite is nevertheless well above the noise, as seen by the presence of well-defined diffraction spots (corresponding to this peak) in

Figure 8 and Figure 9 illustrate the plot of intensity vs. 2θ obtained following manual baseline subtraction of the background intensity and peak-fitting using the Gaussian function. Here *xc* is the peak location (2θ) in °, *w* is a measure of the width of the peak at half its maximum amplitude (in °), and *A* is the total area under the curve from the baseline. The figures show peaks in approximately the same places as indicated in the previous x-ray experiments, and additionally indicate that the peak area is about 5 times lower (for *Ase* A = 0.27518, for *Bse* A = 1.5542) in the *Ase* sample than the *Bse* sample. If dispersion states were identical in both samples, we would expect the peak to be only 2.5 times lower in the *Ase* sample, since there is 2.5 times less material. That the peak is even weaker in the *Ase* sample than one would expect does not prove greater dispersion in the *Ase* sample (since there are other things that could reduce the area of that peak), but it is consistent with greater dispersion in the *Ase* sample.

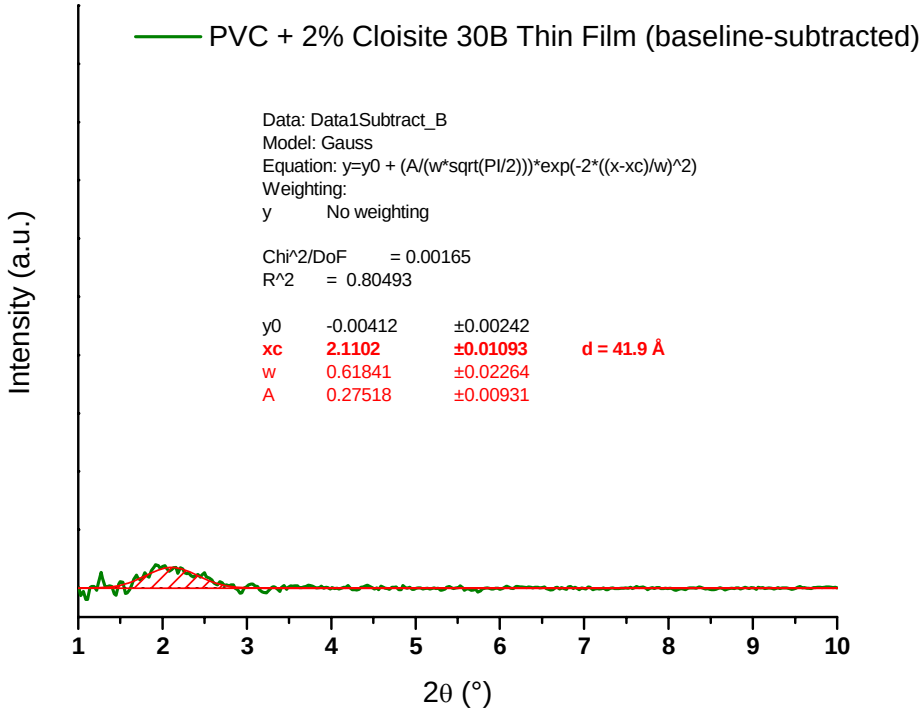

Figure 8. Integrated intensity (arbitrary units) vs. 2θ (°), baseline-subtracted and peak-fit using a Gaussian model, for ***Ase*** nanocomposite sheet

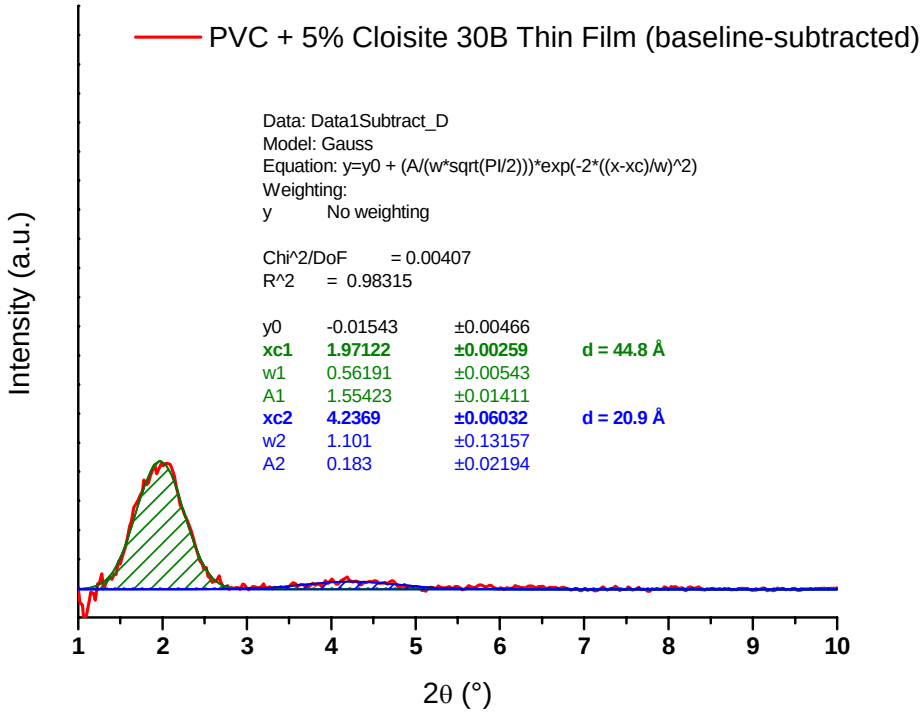

Figure 9. Integrated intensity (arbitrary units) vs. 2θ (°), baseline-subtracted and peak-fit using a Gaussian model, for ***Bse*** nanocomposite sheet

Figure 10 shows azimuthal scans for the same samples, again with Gaussian peak-fits. The strength of the first peak seen in the two-theta scans vs. orientation angle is shown, indicating the degree of orientation of the diffracting (intercalated) clay stacks. Random orientation should give flat plots (continuous rings in the diffraction images) while peaks indicate orientation (bright spots in the diffraction images). The peak locations confirm that the maximum degree of orientation is observed in the plane of the thin films, while their widths indicate that most of the intercalated OMMT seen in XRD is oriented no more than 30° away from the plane of the sample. The peak area for Sample *Bse* containing 5 wt% OMMT is almost exactly 2.5 times larger than the equivalent area for Sample *Ase* containing 2 wt% OMMT (A = 489.04 vs. A = 185.54), just as one would expect based on the OMMT content. This indicates that these samples share a similar dispersion state; that this contradicts the 2θ scans may relate to errors introduced during baseline subtraction or low signal-to-noise ratio.

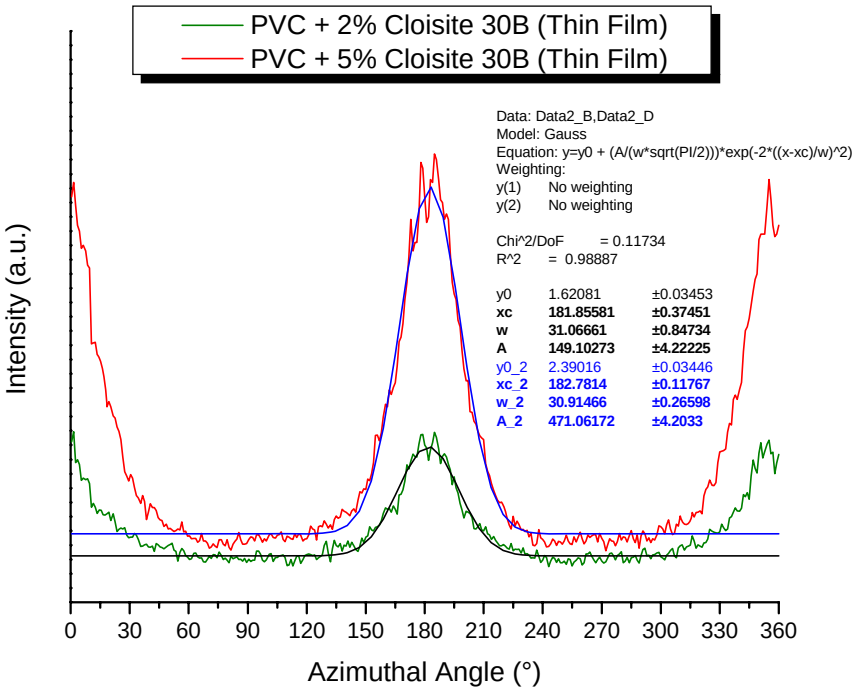

Figure 10. Azimuthal scans for PVC nanocomposite sheets *Ase* and *Bse*

Permeability of PVC / OMMT *Nanocomposites*

Results of barrier properties testing are tabulated in Table 2. A five-fold increase in oxygen barrier is observed in the *Ase* nanocomposite vs. the pure PVC (Sample *Jse*), a substantial improvement and evidence of high levels of OMMT dispersion. In contrast, the *Bse* sample shows higher permeation rates than the *Ase* sample and approaches the permeability of pure PVC. This is attributed to a combination of poorer OMMT dispersion and greater thermal degradation in the *Bse* sample as a direct result of the higher OMMT content.

To expand on this point, the high aspect ratio of the clay layers is such that, when individually dispersed in a matrix, they form a "maze" that diffusing species must navigate. More layers reduce the rate of motion so long as they remain individually dispersed. If the introduction of more layers causes stack formation or agglomeration, however, the number and aspect ratio of discrete particles may decrease even as the total number of layers in the system increases, reducing or reversing improvements in barrier properties. Likewise, the thermal degradation of PVC results in substantial increase in permeability thanks to the formation of and subsequent oxidation and crosslinking of polyacetylene[21, 22] and the associated degradation in properties and reduction in density.

Table 2. Oxygen Permeability Results

Sample ID	Sample Makeup	Thickness	Area	Transmission Rate	Permeation Rate	Average Perm. Rate
		(mm)	(cm^2)	cc/(m^2-day)	cc-mm/(m^2-day)	cc-mm/(m^2-day)
Jse	Pure PVC	0.71	50	124.1	86.8	**88.2**
Jse	Pure PVC	0.74	50	121.1	89.6	
Ase	2 wt% OMMT	0.41	50	43.5	17.6	**17.6**
Ase	2 wt% OMMT	0.4	50	44.5	17.6	
Bse	5 wt% OMMT	0.4	50	175.2	70.1	**69.3**
Bse	5 wt% OMMT	0.39	50	176.4	68.79	

Thermal Analysis (TGA)

The presence of compatible layered silicates in a polymer matrix enhances the formation of char and hinders diffusion of volatile decomposition products in a variety of nanocomposite systems[23, 24, 25, 26]. Consistent with this idea, indications of enhanced thermal stability[7, 8, 11] and flame retardance[27] have been reported in PVC nanocomposites similar to those studied here.

The results of TGA experiments performed in air on pure PVC and its nanocomposites are shown in Figure 11 (curves shifted vertically for clarity, onset temperatures indicated), with derivative curves shown in Figure 12. The peaks in the derivative curves correspond to the temperatures of maximum degradation (as measured by maximum rate of weight loss). The onset and maximum degradation temperatures and residue yield are shown in Table 3.

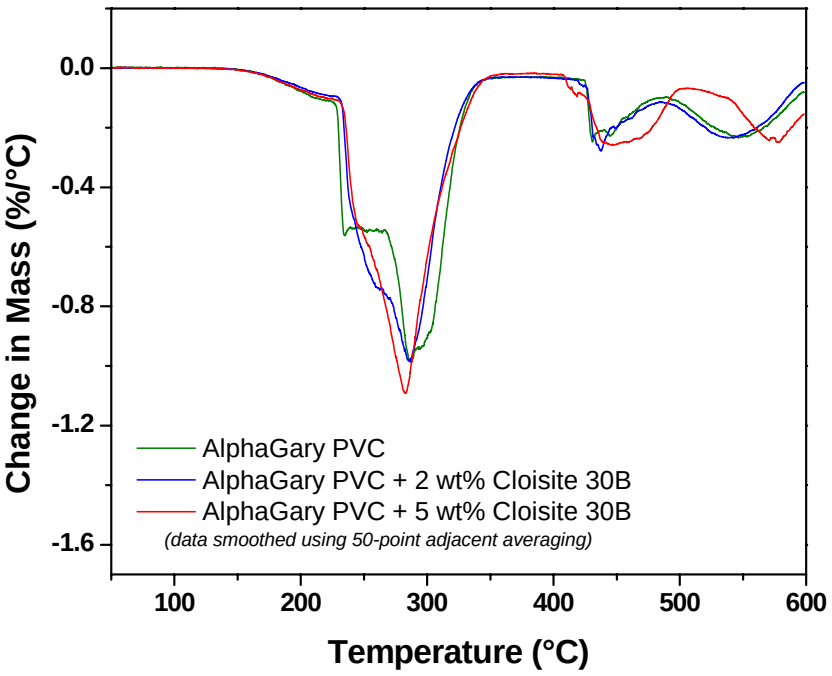

Figure 11. TGA curves for PVC (*Je*, green) and its OMMT nanocomposites (Je, Ae, blue, and Be, red) (shifted vertically for comparison)

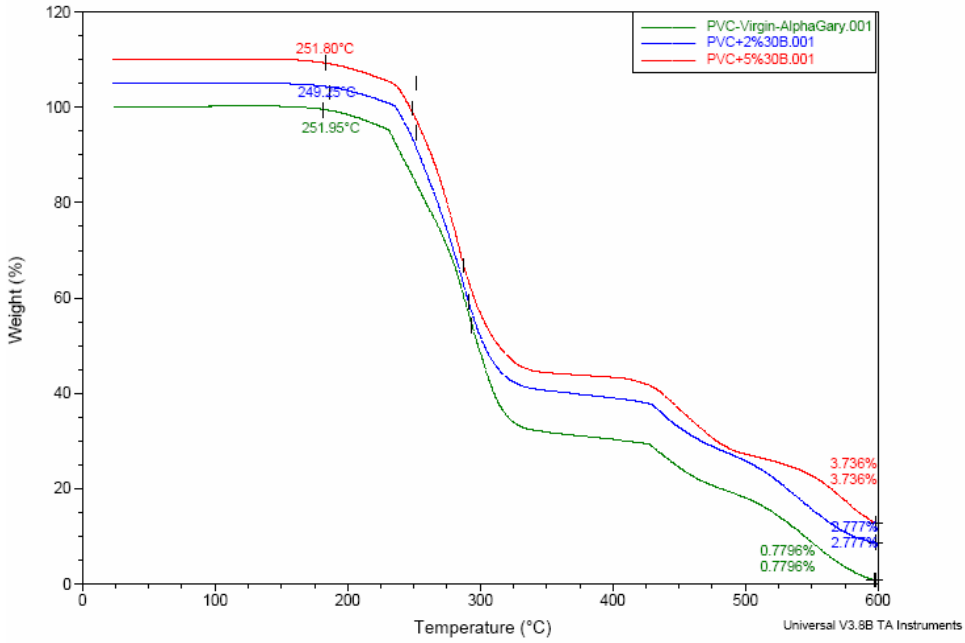

Figure 12. Derivative curves for PVC (*Je*, green) and its OMMT nanocomposites (*Je*, *Ae*, blue, and *Be*, red)

Table 3. TGA Results from PVC and PVC /OMMT Nanocomposites

Sample ID	OMMT content	T_d (onset)	T_d (max.)	Residue at 600 °C (expected)	Residue at 600 °C (actual)
		°C	°C	(wt %)	(wt %)
Je	0	252	287	0	0.8
Ae	2	250	285	1.4	3.7
Be	5	252	283	3.5	2.8

These results indicate that this particular combination of OMMT and PVC resin does not give rise to substantial changes in thermal stability, at least as measured by the TGA analyses reported here. Differences in residue yield are not considered significant and are likely due to incomplete degradation, the presence of inorganic additives such as zinc based thermal stabilizers in the pure PVC, and/or small variations in OMMT content.

With that said, it should be noted that there are many ways of measuring heat stability, and that we have picked a worse case situation here by performing TGA in air. In contrast, the aforementioned studies show enhanced thermal stability via experiments under inert atmosphere[7, 8, 11]. This is significant because oxygen plays an important role in the thermal degradation of organic compounds in general.

At the time of writing the authors are aware of only a single report directly comparing these situations, which shows that most or all of the enhancements in thermal stability as measured by TGA disappears when moving from nitrogen to air[28]. While direct comparisons of degradation temperatures are not possible given substantial differences in composition and processing between our samples and those analyzed in the aforementioned study, our results are consistent in showing minimal effect in the presence of air.

This is an extremely important statement, given that the only other reports we are aware of that attempt to measure thermal degradation of PVC nanocomposites in air via any means indicate *enhanced* thermal degradation in air in the presence of OMMTs[29, 30]. That we do not see such enhancements in our systems based on the TGA data presented here further emphasizes the importance of formulation.

It be emphasized as well that TGA, while a useful tool, is designed by its very nature to reduce or eliminate kinetic effects by slowly heating of a small sample with a high surface to volume ratio. A thicker, more massive piece of electrical insulation exposed to hot but relatively stagnant air in a confined space will not behave in the same way. Here, barrier properties will affect the ability of oxygen to reach material below the surface of the insulation, controlling the degree to which its thermal stability of the underlying material is affected by its presence.

In summary, improved fire retardance[27] is supported by the literature, as is enhanced thermal stability in the absence of oxygen[7, 8, 11]. Two very recent reports show degraded thermal stability in the presence of oxygen[29], while another, like our materials, shows minimal changes[28]. Based on this work, then, we may therefore realize improvements in heat stability in more realistic settings by taking advantage of the substantial improvements in oxygen barrier properties realized in the 2 wt% nanocomposites.

Mechanical Properties

Figure 13 shows tensile specimens from the extruded sheet. Figure 14 shows the testing equipment used for the tensile tests (made according to ASTM D412-98a).

Figure 13. Sample *Ase* cut tensile and Sample *Jse* (virgin PVC) cut tensile (at right).

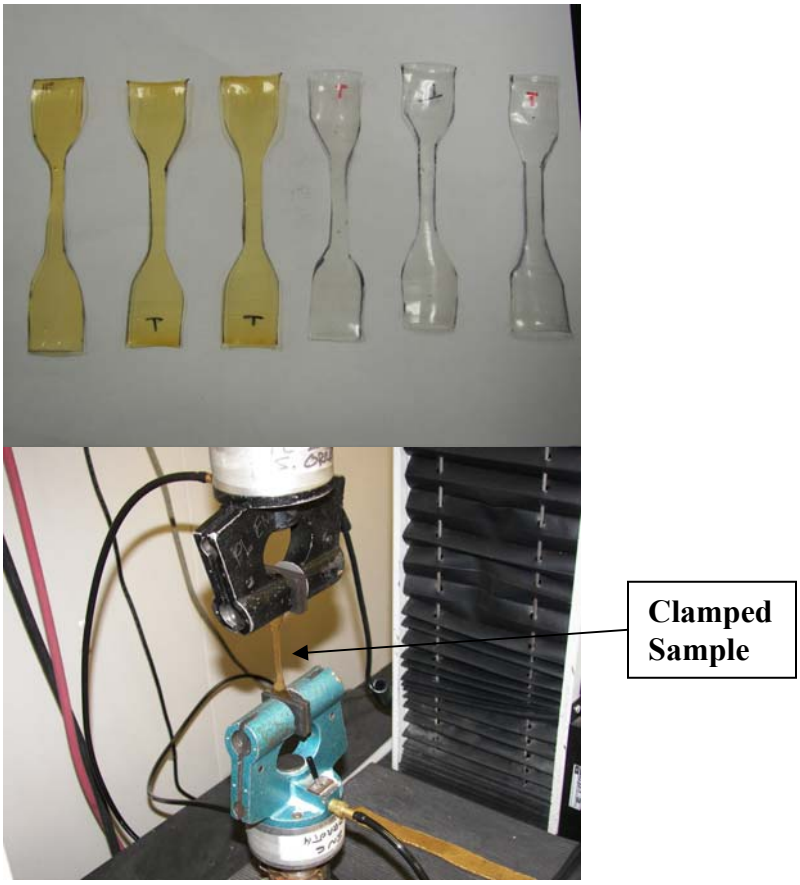

Figure 14. Tensile testing arrangements in the Instron 4400.

Tensile test results from the three compositions tested are given in Table 4, including modulus (which relates to the stiffness of a sample in tension), ultimate elongation (which relates to the ductility of the sample in tension), and ultimate strength (which relates to the strength of the sample in tension).

Table 4. Mechanical Properties of PVC and PVC /OMMT Nanocomposite Extruded Sheet

Sample ID	OMMT Content	Modulus (MPa)		Failure Stress (MPa)		Failure Strain (%)	
		TD	MD	TD	MD	TD	MD
Je	***0 wt%***	***100***	***78***	***23***	***23***	***211***	***244***
	Std. Dev.	*5*	*12*	*6*	*3*	*48*	*65*
Ae	***2 wt%***	***76***	***100***	***18***	***21***	***167***	***223***
	Std.Dev.	*6*	*6*	*6*	*3*	*75*	*63*
Be	***5 wt%***	***131***	***101***	***18***	***17***	***167***	***159***
	Std.Dev.	*7*	*10*	*6*	*3*	*87*	*87*

*(**TD** = Tested in transverse direction, **MD** = Tested in machine [extrusion] direction)*

From these test results we see a rough correlation of modulus with OMMT content. The overall results indicate that 2 wt% loading (Sample *Ase*) is optimal from a mechanical standpoint, however, as at 5 wt% OMMT concentration both failure stress and strain decrease substantially, implying a less ductile, more brittle sample. One explanation for this is enhanced degradation, resulting in polyacetylene formation and its subsequent oxidation and crosslinking[21, 22]; such highly crosslinked materials are brittle by nature. As before it should be noted here that the *Jse* sample virgin PVC has only a single process history, in comparison with the *Ase* and *Bse* samples, both of which were processed twice (twin screw extrusion then sheet extrusion), and that processing encourages degradation in these systems.

Alternatively, microscale dispersion may also play a role, with agglomeration more likely as OMMT content increases. Failure-dependent properties are highly sensitive to flaws like clay agglomerates because they act as stress concentrators within the polymer matrix, leading to crack formation, propagation and failure of the material; even single agglomerates in the wrong place can therefore lead to early failure.

Conclusions

Lead-free PVC/clay nanocomposites have been successfully prepared by the melt blending of PVC with organically modified clay, with their excellent transparency serving as an indicator of clay dispersion[31]. Quantitative structural analyses (via x-ray diffraction) indicate significant intercalation and orientation in the direction of flow of the polymer melt, and allow for the possibility of partial exfoliation.

Consistent with the structure of these nanocomposites, it has been found that the addition of only 2 wt% of OMMT results in a five-fold enhancement in oxygen barrier. While TGA analyses do not indicate improved thermal stability in these nanocomposites, such a significant enhancement in oxygen barrier may nevertheless result in improved thermal and/or fire performance in more realistic situations where oxygen permeation kinetics is more likely to play a role. Finally, tensile testing indicates that 2 wt% is optimal with respect to mechanical properties as well; while modulus tends to increase with clay content, failure stress and strain are reduced. This is likely due to increasing process-induced polymer degradation and the greater probability of agglomerate formation at higher clay contents.

Having confirmed that it is possible to enhance properties relevant to thermal and/or fire stability (i.e. oxygen barrier) with the addition of a small amount of clay and without substantially degrading the mechanical properties in lead-free PVC nanocomposites, additional studies have shown the possibility for the production of PVC/plasticizer masterbatches as a means of further improving clay dispersion levels while reducing dust hazards associated with the clays themselves. While such masterbatches proved to be incompatible with the PVC resin used in this work to date, a major producer of vinyl wire and cable insulation has recently shipped a variety of materials specific to wire and cable formulations that are compatible with the DIDP plasticizer used in these masterbatching studies.

In addition to work to extend these studies into more realistic PVC wire and cable formulations, TGA-FTIR experiments are also planned as a means of studying both the nature of thermal degradation in these materials and also the effect of added clay on plasticizer loss via volatilization. Given that clays may act as plasticizers and allow for reductions in phthalate content[7], the practical reduction and/or replacement of phthalates in these formulations may also be possible.

References

1 For additional discussion see "Environmental, Health and Safety Issues in the Coated Wire and Cable Industry", Technical Report No. 51, prepared by Greiner Environmental, Inc. for UML TURI (http://www.turi.org/content/content/view/full/994/)

2 See http://www.honeywell.com/sites/sm/aegis/ for product descriptions.

3 Image from http://www.specialchem4polymers.com/tc/Tin-Stabilizers/index.aspx?id=2821

4 LeBaron, P. C.; Wang, Z.; Pinnavaia, T. J. "Polymer-layered silicate nanocomposites: an overview" *Applied Clay Science* **15** 11 (1999).

5 Alexandre, M.; DuBois, P. "Polymer-layered silicate nanocomposites: preparation, properties and uses of a new class of materials" *Materials Science and Engineering R: Reports* **28** 1 (2000).

6 Schmidt, D. F.; Shah, D.; Giannelis, E. P. "New advances in polymer/layered silicate nanocomposites" *Current Opinions in Solid State and Materials Science* **6** 205 (2002).

7 Wang, D.; Parlow, D.; Yao, Q.; Wilkie C. "PVC-Clay Nanocomposites: Preparation, Thermal and Mechanical Properties" *Journal of Vinyl & Additive Technology* **7** 203 (2001).

8 Du, J.;Wang, D.;Wilkie, C.; Wang, J. "An XPS investigation of thermal degradation and charring on poly(vinyl chloride)–clay nanocomposites" *Polymer Degradation and Stability* **79** 319 (2003).

9 Kim, Y.; White, J. L. "Melt-Intercalation Nanocomposites with Chlorinated Polymers" *Journal of Applied Polymer Science* **90** 1581 (2003).

10 Yalcin, B.; Cakmak, M. "The role of plasticizer on the exfoliation and dispersion and fracture behavior of clay particles in PVC matrix: a comprehensive morphological study" *Polymer* **45** 6623 (2004).

11 Yoo, Y.; Kim, S-S.; Won, J. C.; Choi, K-Y.; Lee, J. H. "Enhancement of the thermal stability, mechanical properties and morphologies of recycled PVC/clay nanocomposites" *Polymer Bulletin* **52** 373 (2004).

12 Kovarova, L.; Kalendova, A.; Simonik, J.; Malac, J.; Weiss, Z.; Gerard, J. F. "Effect of melt processing conditions on mechanical properties of polyvinylchloride/organoclay nanocomposites" *Plastics, Rubbers and Composites* **33** 287 (2004).

13 Kovarova, L.; Kalendova, A.; Gerard, J. F.; Malac, J.; Simonik, J.; Weiss, Z. "Structure Analysis of PVC Nanocomposites" *Macromolecular Symposia* **221** 105 (2005).

14 Yalcin, B.; Cakmak, M. "Molecular Orientation Behavior of Poly(vinyl chloride) as Influenced by the Nanoparticles and Plasticizer during Uniaxial Film Stretching in the Rubbery Stage" *Journal of Polymer Science B* **43** 724 (2005).

15 Hu, H.; Pan, M.; Li, X.; Shi, X.; Zhang, L. "Preparation and characterization of poly(vinyl chloride)/organoclay nanocomposites by in situ intercalation" *Polymer International* **53** 224 (2004).

16 Refer to http://www.nanoclay.com/keyproperties.asp, http://www.scprod.com/product_bulletins/PB%20Cloisite%2030B.pdf, and http://www.scprod.com/product_bulletins/PB%20Cloisite%2010A.pdf.

17 Kise, H. "Dehydrochlorination of poly(vinyl chloride) by aqueous sodium hydroxide solution under two-phase conditions" *Journal of Polymer Science, Polymer Chemistry Edition* **20** 3189 (1982).

18 Hollaender, A.; Zimmermann, H.; Behnisch, J. "Chemical dehydrochlorination of poly(vinyl chloride). Dehydrochlorination by alkali alkoxides" *European Polymer Journal* **27** 959 (1991).

19 Refer to http://www.scprod.com/product_bulletins/PB%20Cloisite%2030B.pdf

20 Refer to http://www.scprod.com/msds/Cloisite%2030B.pdf

21 Sears, J. K.; Darby, J. R. "Technology of Plasticizers" *John Wiley & Sons* **Ch. 7** Sect. A 583 (1982) [http://www.knovel.com/knovel2/Toc.jsp?BookID=734]

22 Owen E. D., ed. "Degradation and Stabilization of PVC" *Elsevier* (1984).

23 Gilman, J. W. "Flammability and thermal stability studies of polymer layered-silicate clay/nanocomposites" *Applied Clay Science* **15** 31 (1999).

24 Porter, D.; Metcalfe, E.; Thomas, M. J. K. "Nanocomposite Fire Retardants – A Review" *Fire and Materials* **24** 45 (2000).

25 Beyer, G. "Nanocomposites: a new class of flame retardants for polymers" *Plastics Additives & Compounding* **4** 10 (2002).

26 Morgan, A. B. "Flame retarded polymer layered silicate nanocomposites: a review of commercial and open literature systems" *Polymers for Advanced Technologies* **17** 206 (2006).

27 Kalendova, A.; Kovarova, L.; Malac, Z.; Malac, J.; Vaculik, J.; Hrncirik, J.; Simonik, J. "Modified Clay in Polyvinylchloride (PVC)" *Society of Plastics Engineers 60th Annual Technical Conference* **2** 2250 (2002).

28 Gong, F.; Feng, M.; Zhao, C.; Zhang, S.; Yang, M. "Thermal properties of poly(vinyl chloride)/montmorillonite nanocomposites" *Polymer Degradation and Stability* **84** 289 (2004).

29 Peprnicek, T.; Duchet, J.; Kovarova, L.; Malac, J.; Gerard, J. F.; Simonik, J. "Poly(vinyl chloride)/clay nanocomposites: X-ray diffraction, thermal and rheological behaviour" *Polymer Degradation and Stability* **91** 1855 (2006).

30 Ren, T.; Yang, J.; Huang, Y.; Ren, J.; Liu, Y. "Preparation, Characterization, and Properties of Poly(vinyl chloride)/Organophilic-Montmorillonite Nanocomposites" *Polymer Composites* **27** 55 (2006).

31 Bur, A.; Lee, Y.; Roth, S.; Start, P. "Measuring the extent of exfoliation in polymer/clay nanocomposites using real-time process monitoring methods" *Polymer* **46** 10908 (2005).